Journal of Power Sources 205 (2012) 239–243

Contents lists available at SciVerse ScienceDirect

Journal of Power Sources

journal homepage: www.elsevier.com/locate/jpowsour

Short communication

Graphene nanosheets supported hollow Pt&CoSn(OH)$_6$ nanospheres as a catalyst for methanol electro-oxidation

Baomin Luo[a,b], Shan Xu[c], Xingbin Yan[a,*], Qunji Xue[a]

[a] State Key Laboratory of Solid Lubrication, Lanzhou Institute of Chemical Physics, Chinese Academy of Sciences, Lanzhou 730000, PR China
[b] Graduate School of Chinese Academy of Sciences, Beijing 100039, PR China
[c] State Key Laboratory for Oxo Synthesis and Selective Oxidation, Lanzhou Institute of Chemical Physics, Chinese Academy of Sciences, Lanzhou 730000, PR China

ARTICLE INFO

Article history:
Received 21 November 2011
Received in revised form 11 January 2012
Accepted 12 January 2012
Available online 21 January 2012

Keywords:
Graphene
Platinum
Cobalt tin hydroxide
Hollow nanosphere
Methanol oxidation

ABSTRACT

A kind of graphene nanosheets (GNSs) supported hollow composite of Pt and CoSn(OH)$_6$ electro-catalyst (H-Pt&CoSn(OH)$_6$/GNSs) is prepared using cobalt metal nanoparticles as sacrificial templates. Transmission electron microscope measurements show that GNSs supported H-Pt&CoSn(OH)$_6$ nanospheres are coreless with a uniform particle size of 11 nm. Electrochemical measurements demonstrate that the H-Pt&CoSn(OH)$_6$/GNSs electro-catalyst exhibits enhanced electro-catalytic performance for methanol oxidation compared with solid Pt&CoSn(OH)$_6$/GNSs, and Pt/GNSs catalysts.

© 2012 Elsevier B.V. All rights reserved.

1. Introduction

As a cheap liquid fuel, methanol has several advantages over hydrogen. It is very easily handled, transported, stored, and has a high theoretical energy density. Recently, direct methanol fuel cells (DMFCs) had been widely studied for compact, high energy-density power sources. Among various candidates, Pt has stimulated considerable research into its use as a catalyst in DMFC. However, a critical problem for Pt catalyst is the prohibitive cost. Therefore, economical and effective alternative catalysts are required and cost-effective routes are being sought to make more efficient Pt catalysts for DMFCs. One approach is to employ bi- or tri-metallic catalysts that combine Pt with other metals such as Ru, Fe, Ni, Co, Sn, etc. [1–5]. Incorporation non-precious metals into the catalysts nanostructure not only enhances catalytic activity and but also improves stability. The enhanced activity and stability are usually interpreted in terms of a bifunctional mechanism. The whole mechanism in the case of PtRu catalyst can be shown as follows:

$$Pt + CH_3OH = Pt{-}CO + 4H^+ + 4e^- \quad (1)$$

$$Ru + H_2O = Ru{-}OH + H^+ + e^- \quad (2)$$

$$Ru{-}OH + Pt{-}CO = Ru + Pt + CO_2 + H^+ + e^- \quad (3)$$

Pt is easily subjected to CO poison, an intermediate of methanol oxidation although Pt is the most active catalyst of all metallic catalysts for methanol oxidation. So, it is necessary to remove CO from the surface of platinum, especially at a relatively negative potential. Adding Ru into Pt catalysts has been known to be significantly effective for CO removal at a relatively negative potential. Ru sites adsorb oxygen-containing species at a potential of 0.2–0.3 V lower than the pure Pt sites, which promotes the oxidation of CO into CO_2, thus providing more active Pt sites for methanol oxidation [6–9]. Both PtSn and PtCo have been reported to be promising catalysts for methanol oxidation. Similarly, the Sn and Co atoms in PtSn and PtCo catalysts can also adsorb oxygen-containing species to form Sn—OH and Co—OH. The forming products can initiate the oxidation of adsorbed CO on Pt cites at lower potentials as compared to Pt [10–12].

In recent years, hollow metal nanostructures have captured the attention of researchers due to the increased surface area, low density, cost-saving of material, which make them exhibit catalytic activities different from their solid counterparts [13–15,12,16]. In commonly used methods, materials with hollow nanostructures are usually fabricated by using a sacrificial template, such as silica spheres [17,18] or polystyrene spheres [19,20] followed by the removal of the template, which made the process complicated and limited their use. The galvanic replacement reactions involving desired metal ions and sacrificial metal nanoparticles provide a simple route to the facile synthesis of hollow noble metal nanostructures. For example, hollow Pt [13], Au [21], Pd [22], AuPt alloy

* Corresponding author. Tel.: +86 931 4968055; fax: +86 931 4968055.
E-mail address: xbyan@licp.cas.cn (X. Yan).

0378-7753/$ – see front matter © 2012 Elsevier B.V. All rights reserved.
doi:10.1016/j.jpowsour.2012.01.077

[23], CoPt alloy [12], PtPd [24] and PtRu [25] nanostructures have been prepared in this way, in which Co nanoparticles are sacrificed as the templates in the replacement reactions. However, hollow PtSn cannot be prepared by this method because Sn ion cannot be reduced by Co metal. To realize the reduction of Sn ion, reducing agent should be enough to reduce Sn ion. Some Co metal will exist in final product, and a hollow PtSnCo ternary system will be formed.

On the other hand, it has been proved that supported metal nanoparticles show higher electro-catalytic activity and utilization efficiency compared with unsupported metal particles because of their large surface area and high dispersion on the supports [26]. Up to now, various kinds of carbon materials, including activated carbon, porous carbon, carbon aerogels, carbon fibers and carbon nanotubes, have been widely used as the catalyst supports in DMFCs. Graphene nanosheet (GNS), a new two-dimensional carbon material with single (or a few) atomic thickness, has recently attracted an enormous amount of interest from both theoretical and experimental scientists due to their potential applications, such as lithium ion batteries [27–29] and electrochemical capacitors [30,31]. Moreover, the combination of its high surface area (theoretical value of 2630 $m^2\ g^{-1}$), high conductivity, unique graphitized basal plane structure and potential low manufacturing cost makes it a promising candidate for catalyst support in DMFCs [32–41]. It has been proved that catalysts supported on GNSs show improved activity than those supported on carbon black [32,36–41].

In this communication, we design a facile route based on the replacement reaction to synthesize GNSs supported hollow PtSnCo ternary system. It is interesting that the product is not PtSnCo ternary alloy but a composite of Pt and $CoSn(OH)_6$. To the best of our knowledge, it is the first time to fabricate hollow composite of Pt and $CoSn(OH)_6$ nanosperes. Furthermore, as-prepared GNSs supported hollow composite of Pt and $CoSn(OH)_6$ nanosperes (H-Pt&$CoSn(OH)_6$/GNSs) exhibits improvement of electro-oxidation activity for CH_3OH in comparison to GNSs supported solid composite of Pt and $CoSn(OH)_6$ catalyst (S-Pt&$CoSn(OH)_6$/GNSs), pure Pt catalyst (Pt/GNSs), carbon black supported H-Pt&$CoSn(OH)_6$ (H-Pt&$CoSn(OH)_6$/C) catalyst, and commercial E-tek PtRu/C catalyst.

2. Experimental

2.1. Materials

5 wt% nafion solutions were purchased from Sigma. Graphite powder (325 mesh) was purchased from Qingdao Huatai Tech. Co., Ltd. Carbon black (Vulcan, XC-72R) was provided by Cabot Crop. Other reagents were commercially available and of analytical reagent grade. Deionized water (DI water) with resistance of approximately 18 MΩ cm was used throughout the experiment.

2.2. Preparation of graphene oxide

Graphene oxide (GO) was prepared from natural graphite using modified Hummers' method [40].

2.3. Preparation of the H-Pt&$CoSn(OH)_6$/GNSs catalyst

The H-Pt&$CoSn(OH)_6$/GNSs catalyst was prepared by a two-step method. In a typical synthesis, 40 ml of 0.4 mM $CoCl_2$ and 140 mg of trisodium citrate dihydrate which was used as a stabilizer were mixed in 100 g of DI water. The solution was purged with N_2 for 15 min, then 40 ml of 80 mM $NaBH_4$ was added dropwise into the above solution under vigorous stir, giving rise to a brown Co hydrosol. The Co hydrosol was aged for 1 h. Then, a mixture of 8.3 ml of 19.3 mM H_2PtCl_6 and 40 ml of 4 mM $SnCl_2$ was added dropwise under vigorous stir. The color of the solution became black gradually. The $PtCl_6^{2-}$ was reduced to Pt by Co nanoparticles and Co was oxidized to Co^{2+}, forming a hollow nanostructure. The Sn^{2+} and generated Co^{2+} were reduced by $NaBH_4$. We cannot rule out that part of $PtCl_6^{2-}$ was also reduced by $NaBH_4$. The mixture was stirred for 1 h to complete the reaction. To avoid the oxidation of the Co by atmospheric oxygen, high-purity nitrogen was bubbled through the solution during the above procedure. Then, 45 g 0.1 wt% GO was added and the mixture stirred for one night. The product was collected by centrifugation and washed several times with DI water. In order to convert GO to GNSs, the product was solved in 45 g DI water and 45 g 1 wt% fresh $NaBH_4$ solution was added under stir. After stirred for one night, the product was collected by filtration and washed several times with DI water. Finally, the product was dried in a vacuum freeze drier. For the sake of comparison, the S-Pt&$CoSn(OH)_6$/GNSs catalyst was also prepared. In brief, 100 g of DI water, 140 mg of trisodium citrate dihydrate, 8.3 ml of 19.3 mM H_2PtCl_6, 40 ml of 4 mM $SnCl_2$ and 40 ml of 0.4 mM $CoCl_2$ were mixed in 100 g of DI water to form a solution. Then 40 ml of 80 mM $NaBH_4$ was added dropwise into the above solution under vigorous stirring. The procedures of mixing the above solution with GO and converting GO to GNSs were the same as those in the preparation of H-Pt&$CoSn(OH)_6$/GNSs catalyst. The H-Pt&$CoSn(OH)_6$/C was also prepared. The procedures for preparation H-Pt&$CoSn(OH)_6$ was the same as preparation of H-Pt&$CoSn(OH)_6$/GNSs. The prepared H-Pt&$CoSn(OH)_6$ are mixed with carbon black by magnetic stirring. The product was collected by filtration and washed several times with DI water. Finally, the product was dried in a vacuum freeze drier. Moreover, a Pt/GNSs catalyst was also prepared (The prepared procedure presented in our previous work [40]).

2.4. Characterization

Structural and morphological investigations of the samples were performed by X-ray diffraction using Cu Kα radiation (XRD, Panalytical X' Pert Pro) and transmission electron microscope (TEM, Tecnai-G2-F30). An IRIS Advantage ER/S inductively coupled plasma spectrometer (ICP, TJA) was used for all metal-determinations. The surface chemical species of H-Pt&$CoSn(OH)_6$/GNSs were examined using a Perkin-Elmer PHI-5702 multifunctional X-ray photoelectron spectroscope (XPS, Physical Electronics) with Al Ka radiation of 1486.6 eV as the excitation source.

2.5. Electrochemical measurements

Cyclic voltammetry (CV) and chronoamperometry (CA) measurements were performed with a μAutolab III electrochemical workstation at room temperature. As a typical process, 5 mg of catalyst was ultrasonically mixed with 2 ml of ethanol to form a homogeneous ink, 10 μl of this ink was dropped onto the surface of a glass carbon electrode (GCE, 3 mm in diameter), and then 3 μl of diluted nafion solution (5 wt% nafion solution was diluted by 10 times ethanol by volume) was dropped to fix the catalyst sample on the electrode. Pt wire and a saturated calomel electrode (SCE) were used as counter electrode and reference electrode, respectively. The activity of the catalysts for methanol oxidation reaction was measured in a 0.5 M H_2SO_4 + 1.0 M CH_3OH aqueous solution at a scan rate of 50 mV s^{-1}. CA tests were carried out at 0.4 V for 7200 s.

3. Results and discussion

3.1. Characterizations of the catalysts

Fig. 1 shows the TEM images of the samples. The TEM image of Pt/GNSs shows that the Pt nanoparticles are uniformly deposited

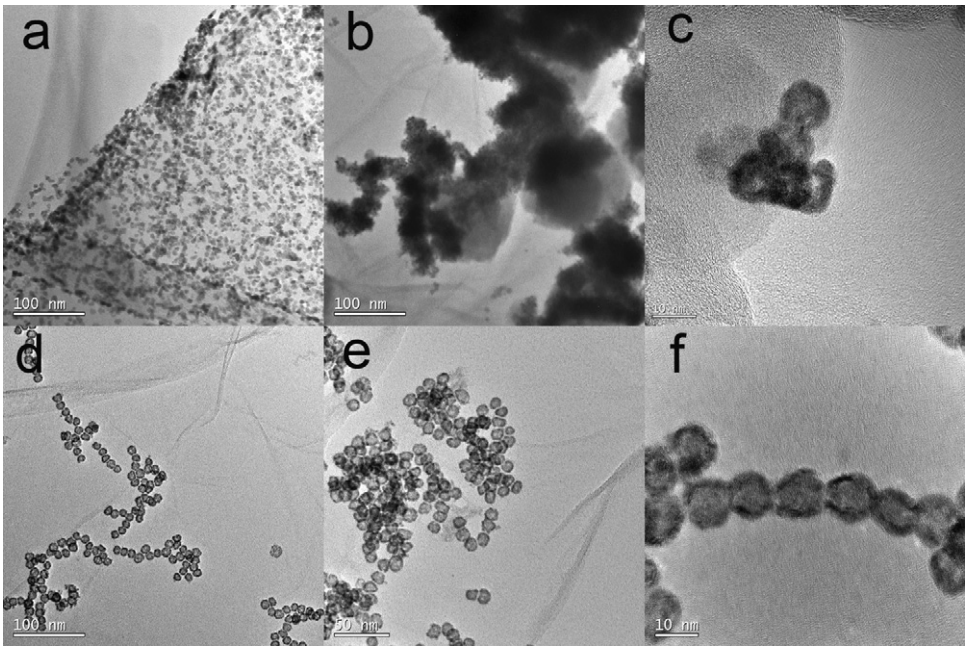

Fig. 1. TEM images of (a) the Pt/GNSs catalyst, (b) the S-Pt&CoSn(OH)$_6$/GNSs catalyst, (c) the H-Pt&CoSn(OH)$_6$/C catalyst, (d and e) the H-Pt&CoSn(OH)$_6$/GNSs catalyst, and (f) hollow tube-like structure of the H-Pt&CoSn(OH)$_6$/GNSs catalyst.

on GNSs with a particle size of 4.8 nm (Fig. 1a). Fig. 1b shows the image of S-Pt&CoSn(OH)$_6$/GNSs catalyst. It can be seen that the catalyst are not spherical but cluster structure. Fig. 1c shows the TEM images of H-Pt&CoSn(OH)$_6$/C catalyst. It can be seen that the nanoparticles supported on carbon black are coreless. Fig. 1d and e shows TEM images of H-Pt&CoSn(OH)$_6$/GNSs catalyst. It can be seen that the particles are spherical with uniform particle size. In addition, the nanospheres centers are brighter than the edges, indicating a hollow nanostructure. The average diameter of the nanospheres is approximately 11 nm. This value is smaller than those of the hollow nanoparticles which are prepared using the same method [12,13,24,25]. Moreover, because the nanoparticles are coreless (hollow), the thickness of shells is very thin and some shells are open, the specific surface area is much larger than that of solid nanoparticles with the same diameter. It also can be seen that the hollow nanospheres are supported on GNSs, indicating the H-Pt&CoSn(OH)$_6$/GNSs catalyst is formed. There are some wrinkles on GNSs, which are the typical morphological feature of GNSs. Moreover, it is interesting that some hollow nanospheres link into 1-dimentional tube-like structure (Fig. 1f). Liang et al. observed the same structure in their prepared hollow AuPt nanospheres [23]. The mechanism for the formation of 1-D nanomaterials is proposed as follows: Co nanoparticles are considerably smaller than the theoretical critical single domain diameter (ca. 55 nm), such that single domain behavior is possible [42]. All the atomic magnetic spins of the nanoparticles are coupled in the same direction, and the nanoparticle behaves as a single magnetic dipole. These nanoparticles are ferromagnetic at room temperature as indicated in the literature [43], thus magnetic interactions among them play a crucial role. The role that citrate play as capping agents is related to the adsorption of citric ions on the Co nanoparticle surface, preventing the growth of Co nanoparticles through double layer repulsion between negatively charged cobalt nanoparticles. When there is not enough citrate, the dipole-dipole interactions are stronger than the repulsive steric interactions caused by citrate. These ferromagnetic nanoparticles are prone to aggregate to form chain-like 1-D nanomaterials to minimize the magnetostatic energy. The Co nanochains will be oxidized by $PtCl_6^{2-}$ to form hollow nanotubes.

Powder XRD patterns of the samples are shown in Fig. 2. The peaks at 40.3, 46.8, and 67.7 are due to the diffractions of Pt (1 0 0), (1 1 0), and (2 1 0) planes. The broad diffraction peak observed around $2\theta = 24^\circ$ is due to the hexagonal structure of GNSs [40]. The patterns of S-Pt&CoSn(OH)$_6$/GNSs (Fig. 2b), H-Pt&CoSn(OH)$_6$/C (Fig. 2c), H-Pt&CoSn(OH)$_6$/GNSs (Fig. 2d) show peaks at 2θ values around 19.8, 23.0, 32.6, 36.7, 38.5, 53.0, and 58.5° are indexed to the diffractions of CoSn(OH)$_6$ (1 1 1), (2 0 0), (2 2 0), (3 1 0), (3 1 1), (4 2 0), and (4 2 2) planes, respectively (JCPDS, no. 13-0356). The average particle sizes of the catalysts were calculated from broadening of the (1 0 0) diffraction peaks using Scherrer's equation. The particle sizes for Pt/GNSs, S-Pt&CoSn(OH)$_6$/GNSs, H-Pt&CoSn(OH)$_6$/C and H-Pt&CoSn(OH)$_6$/GNSs are 5.36, 4.5, 4.1 and 4.1 nm, respectively. It should be noted that the crystallite size are

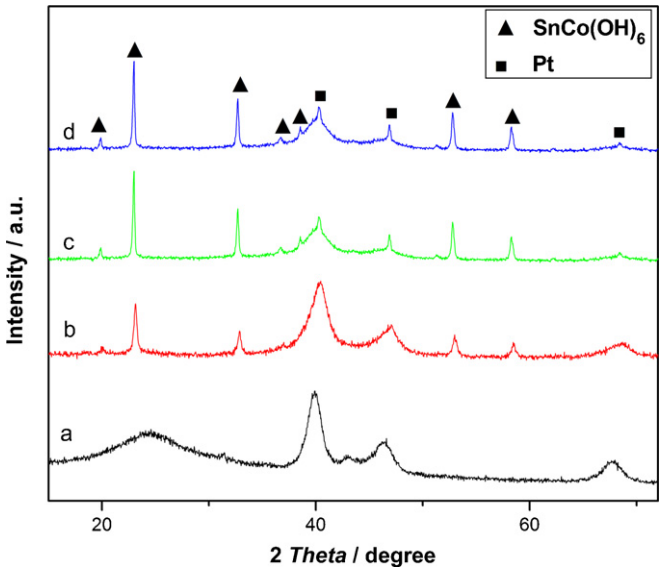

Fig. 2. XRD patterns of (a) the Pt/GNSs catalyst, (b) the S-Pt&CoSn(OH)$_6$/GNSs catalyst, (c) the H-Pt&CoSn(OH)$_6$/C and (d) the H-Pt&CoSn(OH)$_6$/GNSs catalyst.

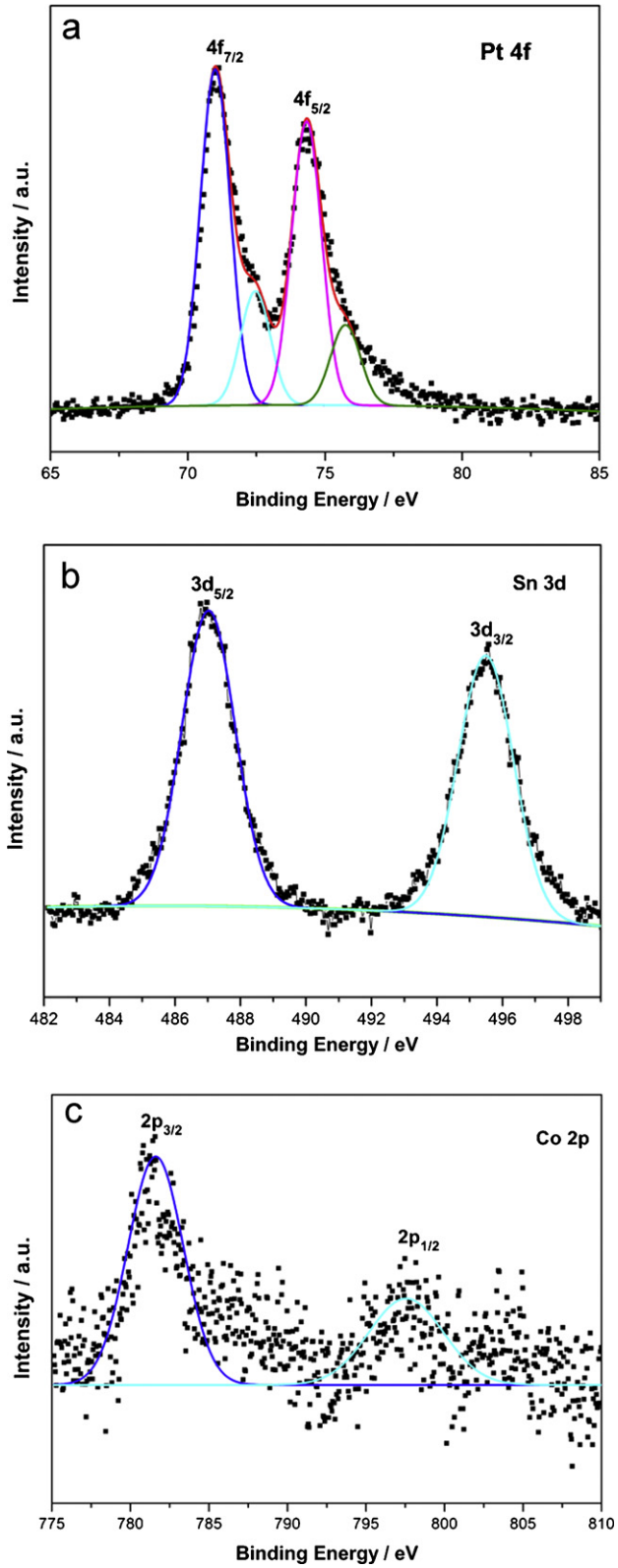

Fig. 3. XPS spectra of the (a) Pt 4f, (b) the Sn 3d, and (c) the Co 2p for the H-Pt&CoSn(OH)$_6$/GNSs catalyst.

hard to accurately calculate due to the disturbing between neighboring diffraction peaks.

Fig. 3a shows the Pt 4f region of the spectrum, which could be deconvoluted into two pairs of doublets. The most intense doublet (at 71.0 and 74.3 eV) is the signature of metallic Pt. The second

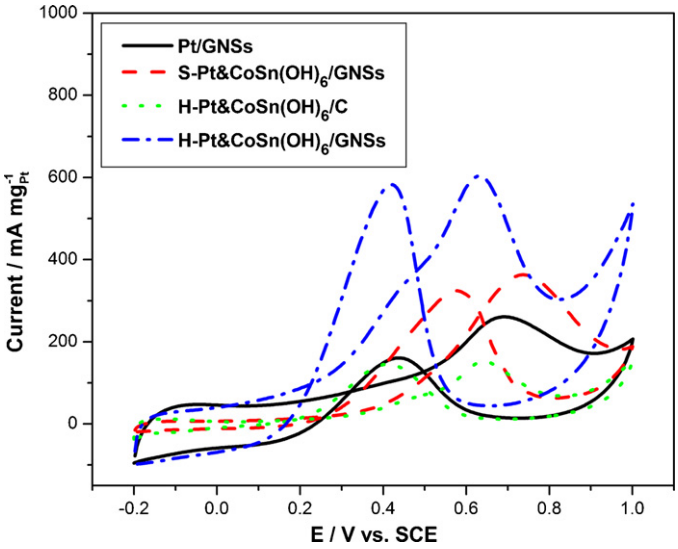

Fig. 4. CVs of the Pt/GNSs catalyst, S-Pt&CoSn(OH)$_6$/GNSs catalyst, H-Pt&CoSn(OH)$_6$/C catalyst and H-Pt&CoSn(OH)$_6$/GNSs catalyst in 0.5 M H_2SO_4 + 1.0 M CH_3OH aqueous solution.

and weaker doublet (at 72.5 and 75.8 eV), with binding energy at 1.5 eV higher than Pt(0), could be assigned to the Pt(II) oxidation state, such as PtO and Pt(OH)$_2$ [44]. Fig. 3b and c shows the Sn 3d region and Co 2p region, respectively. The Sn 3d signals at 487.0 and 495.5 eV are ascribed to Sn(IV) [45], and the Co 2p signals at 781.0 and 797.0 eV are ascribed to Co(II) [46]. It can be seen that the XPS results are agreement with the XRD results.

3.2. Electrochemical properties of the catalysts

The CVs of the catalysts measured in 0.5 M H_2SO_4 + 1 M CH_3OH is shown in Fig. 4. The oxidation currents have been normalized to mass-specific current density so that the current density can be directly used to compare the catalytic activity of the catalysts. The forward scan peak current density on H-Pt&CoSn(OH)$_6$/GNSs catalyst is 603 mA mg_{Pt}^{-1}, which is larger than that on S-Pt&CoSn(OH)$_6$/GNSs (360 mA mg_{Pt}^{-1}), Pt/GNSs (260 mA mg_{Pt}^{-1}) and H-Pt&CoSn(OH)$_6$/C catalyst (156 mA mg_{Pt}^{-1}). Moreover, the forward scan peak current density on H-Pt&CoSn(OH)$_6$/GNSs catalyst is also larger than that on commercial E-tek PtRu/C catalyst (180 mA mg_{Pt}^{-1}) reported in literature [47]. The H-Pt&CoSn(OH)$_6$/GNSs electro-catalyst show enhanced activity than H-Pt&CoSn(OH)$_6$/C, indicating GNSs is superior to carbon black as support. Sharma et al. believed that the oxygen-containing groups on GNSs improve the wettability and accessibility of methanol to the electroactive surface. GNSs display sufficient conductivity and interaction with Pt catalysts for facilitating charge transport. Moreover, they also reported that oxygen-containing groups on GNSs can promote the oxidation of CO adsorbed, CO_{ads}, on the active Pt sites via the bifunctional mechanism [32]. The H-Pt&CoSn(OH)$_6$/GNSs catalyst and S-Pt&CoSn(OH)$_6$/GNSs catalyst exhibit much better electro-catalytic performance for methanol oxidation than that on Pt/GNSs catalysts. Thus, it is believed that the CoSn-OH species play an important role for determining the electro-catalytic performance. The CoSn-OH species are effective for removing CO from Pt surface and easing off CO poison of Pt. It is believed that the Pt-SnCo(OH)$_6$ and PtSnCo are really playing the same function. The H-Pt&CoSn(OH)$_6$/GNSs electro-catalyst shows enhanced activity than S-Pt&CoSn(OH)$_6$/GNSs electro-catalyst, indicating H-Pt&CoSn(OH)$_6$ is superior to S-Pt&CoSn(OH)$_6$. The enhanced activity is partly due to the hollow structure which increases specific surface area of catalyst.

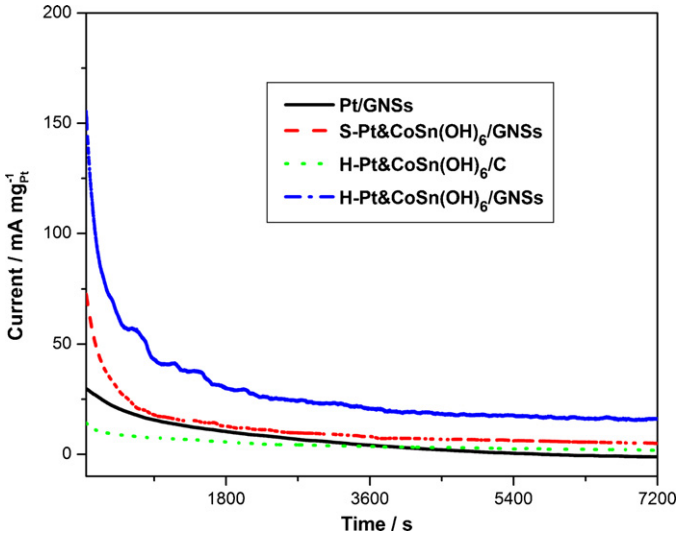

Fig. 5. CAs of the Pt/GNSs catalyst, S-Pt&CoSn(OH)$_6$/GNSs catalyst, H-Pt&CoSn(OH)$_6$/C catalyst and H-Pt&CoSn(OH)$_6$/GNSs catalyst in 0.5 M H_2SO_4 + 1.0 M CH_3OH aqueous solution.

The stability of the samples was tested by CA and the corresponding results are shown in Fig. 5. All catalysts display an initial fast current decay, which is attributed to the poisoning of the catalysts by intermediate species such as CO_{ads}, CH_3OH_{ads}, and CHO_{ads} formed during the methanol oxidation reaction [48]. The steady-state current density on the H-Pt&CoSn(OH)$_6$/GNSs catalyst is the highest during the whole testing time, indicating that the H-Pt&CoSn(OH)$_6$/GNSs catalyst has excellent electro-catalytic activity towards the electro-oxidation of methanol. Meanwhile, the current on the H-Pt&CoSn(OH)$_6$/GNSs catalyst shows long-term stability, indicating it possesses good tolerance towards reaction intermediates and favors long-term application as the anode materials in DMFCs.

4. Conclusion

A facile synthesis of GNSs supported hollow composite of Pt and CoSn(OH)$_6$ electro-catalysts is realized by using Co nanoparticles as sacrificial templates. The GNSs supported H-Pt&CoSn(OH)$_6$ exhibit a superior electro-catalytic activity and stability towards methanol oxidation compared with GNSs supported S-Pt&CoSn(OH)$_6$ electro-catalysts and pure Pt, and carbon black supported H-Pt&CoSn(OH)$_6$.

Acknowledgements

This work was supported by the Top Hundred Talents Program of Chinese Academy of Sciences and the National Nature Science Foundations of China (51005225 and 21103205).

References

[1] K. Park, J. Choi, B. Kwon, S. Lee, Y. Sung, J. Phys. Chem. B 106 (2002) 1869.
[2] Z. Liu, J.Y. Lee, W. Chen, M. Han, L.M. Gan, Langmuir 20 (2004) 181.
[3] J. Xu, K. Hua, G. Sun, C. Wang, X. Lv, Y. Wang, Electrochem. Commun. 8 (2006) 982.
[4] D. Guo, S. Cui, J. Colloid Interf. Sci. 340 (2009) 53.
[5] Z. Liu, B. Guo, L. Hong, T.H. Lim, Electrochem. Commun. 8 (2006) 83.
[6] N.Y. Hsu, C.C. Chien, K.T. Jeng, Appl. Catal. B: Environ. 84 (2008) 196.
[7] D. Chu, S. Gilman, J. Electrochem. Soc. 143 (1996) 1685.
[8] P.W. Albers, W. Weber, K. Kunzmann, M. Lopez, S.F. Parker, Surf. Sci. 602 (2008) 3611.
[9] Z.L. Liu, X.Y. Ling, J.Y. Lee, X.D. Su, L.M. Gan, J. Mater. Chem. 13 (2003) 3049.
[10] A. Bonesi, G. Garaventa, W.E. Triaca, A.M.C. Luna, Int. J. Hydrogen Energy 33 (2008) 3499.
[11] Y. Morimoto, E.B. Yeager, J. Electroanal. Chem. 441 (1998) 77.
[12] D. Guo, S. Cui, J. Power Sources 340 (2009) 53.
[13] Han. Liang, H. Zhang, J. Hu, Y. Guo, L. Wan, C. Bai, Angew. Chem. Int. Ed. 43 (2004) 1540.
[14] Y. Sun, Y. Xia, Science 298 (2002) 2176.
[15] X. Zhou, R. Zhang, Z. Zhou, S. Sun, J. Power Sources 196 (2011) 5844.
[16] G. Chen, D. Xia, Z. Nie, Z. Wang, L. Wang, L. Zhang, J. Zhang, Chem. Mater. 19 (2007) 1840.
[17] L. Lu, H. Zhang, G. Sun, S. Xi, H. Wang, X. Li, X. Wang, B. Zhao, Langmuir 19 (2003) 9490.
[18] J. Park, Y. Kim, C. Oh, S. Shin, Y. Kim, S. Oh, S. Kong, Mater. Res. Bull. 40 (2005) 271.
[19] J. Zhang, J. Liu, S. Wang, P. Zhan, Z. Wang, N. Ming, Ad. Funct. Mater. 14 (2004) 1089.
[20] V.G. Pol, H. Grisaru, A. Gedanken, Langmuir 21 (2005) 3635.
[21] J. Wei, X. Wang, Y. Wang, Q. Chen, F. Pei, Y. Wang, Int. J. Hydrogen Energy 34 (2009) 3360.
[22] J. Ge, W. Xing, X. Xue, C. Liu, T. Lu, J. Liao, J. Phys. Chem. C 111 (2007) 17305.
[23] H. Liang, Y. Guo, H. Zhang, J. Hu, L. Wan, C. Bai, Chem. Commun. (2004) 1496.
[24] B. Liu, H. Li, L. Die, X. Zhang, Z. Fan, J. Chen, J. Power Sources 186 (2009) 62.
[25] D. Guo, L. Zhao, X. Qiu, L. Chen, W. Zhu, J. Power Sources 177 (2008) 334.
[26] N. Chakroune, G. Viau, S. Ammar, L. Poul, D. Veautier, M.M. Chehimi, C. Mangeney, F. Villain, F. Fievet, Langmuir 21 (2005) 6788.
[27] P. Lian, X. Zhu, S. Liang, Z. Li, W. Yang, H. Wang, Electrochim. Acta 55 (2010) 3909.
[28] P. Lian, X. Zhu, S. Liang, Z. Li, W. Yang, H. Wang, Electrochim. Acta 56 (2011) 4532.
[29] Y.J. Mai, X.L. Wang, J.Y. Xiang, Y.Q. Qiao, D. Zhang, C.D. Gu, J.P. Tu, Electrochim. Acta 56 (2011) 2306.
[30] X. Yan, J. Chen, J. Yang, Q. Xue, P. Miele, ACS Appl. Mater. Inter. 2 (2010) 2521.
[31] W. Liu, X. Yan, J. Lang, Q. Xue, J. Mater. Chem. 21 (2011) 13205.
[32] S. Sharma, A. Ganguly, P. Papakonstantinou, X. Miao, M. Li, J.L. Hutchison, M. Delichatsios, S. Ukleja, J. Phys. Chem. C 114 (2010) 19459.
[33] N. Shang, P. Papakonstantinou, P. Wang, S.R.P. Silva, J. Phys. Chem. C 114 (2010) 15837.
[34] S. Wang, S. Jiang, X. Wang, Electrochim. Acta 56 (2011) 3338.
[35] Y. Zhao, L. Zhan, J. Tian, S. Nie, Z. Ning, Electrochim. Acta 56 (2011) 1967.
[36] E. Yoo, T. Okata, T. Akita, M. Kohyama, J. Nakamura, I. Honma, Nano Lett. 9 (2009) 2255.
[37] L. Dong, R.R.S. Gari, Z. Li, M.M. Craig, S. Hou, Carbon 48 (2010) 781.
[38] Y. Li, L. Tang, J. Li, Electrochem. Commun. 11 (2009) 846.
[39] L. Wang, C. Tian, H. Wang, Y. Ma, B. Wang, H. Fu, J. Phys. Chem. C 114 (2010) 8727.
[40] B. Luo, X. Yan, S. Xu, Q. Xue, Electrochim. Acta 59 (2012) 429.
[41] Y. Xin, J. Liu, Y. Zhou, W. Liu, J. Gao, Y. Xie, Y. Yin, Z. Zou, J. Power Sources 196 (2011) 1012.
[42] T. Thurn-Albrecht, J. Schotter, G.A. Kästle, N. Emley, T. Shibauchi, L. Krusin-Elbaum, K. Guarini, C.T. Black, M.T. Tuominen, T.P. Russell, Science 290 (2000) 2126.
[43] Y. Kobayashi, M. Horie, M. Konno, B. Rodríguez-González, L.M. Liz-Marzán, J. Phys. Chem. B 107 (2003) 7420.
[44] F. Liu, J.Y. Lee, W. Zhou, J. Phys. Chem. B 108 (2004) 17959–17963.
[45] A. Lewera, P.J. Barczuk, K. Skorupska, K. Miecznikowsk, M. Salamonczyk, P.J. Kulesza, J. Electroanal. Chem. 662 (2011) 93.
[46] F. Nacimiento, R. Alcántara, U.G. Nwokeke, J.R. González, J.L. Tirado, Ultrason. Sonochem. 19 (2012) 352.
[47] H. Wang, C. Xu, F. Cheng, M. Zhang, S. Wang, S.P. Jiang, Electrochem. Commun. 10 (2008) 1575.
[48] A. Kabbabi, R. Faure, R. Durand, B. Beden, F. Hahn, J.M. Leger, C. Lamy, J. Electroanal. Chem. 444 (1998) 41.